Acta Pharmaceutica Sinica B 2024;14(10):4329–4344

Chinese Pharmaceutical Association
Institute of Materia Medica, Chinese Academy of Medical Sciences

Acta Pharmaceutica Sinica B

www.elsevier.com/locate/apsb
www.sciencedirect.com

ORIGINAL ARTICLE

Ribonucleotide reductase small subunit M2 promotes the proliferation of esophageal squamous cell carcinoma cells *via* HuR-mediated mRNA stabilization

Jing Zhang[a,b,†], Qiong Wu[a,b,†], Yifei Xie[a,b,c], Feng Li[f], Huifang Wei[a,b], Yanan Jiang[a,b], Yan Qiao[a], Yinhua Li[f], Yanan Sun[a,b], Han Huang[a,b], Mengmeng Ge[b], Dengyun Zhao[a,b], Zigang Dong[a,b,c,d,e,*], Kangdong Liu[a,b,c,d,e,*]

[a]*Pathophysiology Department, School of Basic Medical Sciences, Zhengzhou University, Zhengzhou 450000, China*
[b]*China-US (Henan) Hormel Cancer Institute, Zhengzhou 450000, China*
[c]*Tianjian Laboratory for Advanced Biomedical Sciences, Zhengzhou 450052, China*
[d]*State Key Laboratory of Esophageal Cancer Prevention and Treatment, Zhengzhou 450000, China*
[e]*Cancer Chemoprevention International Collaboration Laboratory, Zhengzhou 450000, China*
[f]*The First Affiliated Hospital of Zhengzhou University, Zhengzhou 450000, China*

Received 23 April 2024; received in revised form 11 June 2024; accepted 23 July 2024

KEY WORDS

Esophageal squamous cell carcinoma (ESCC);
Bifonazole;
Ribonucleotide reductase small subunit M2 (RRM2);
AU-rich elements (AREs);
Hu antigen R (HuR);
mRNA stability;
dNTP;

Abstract Esophageal squamous cell carcinoma (ESCC), a malignancy of the digestive system, is highly prevalent and the primary cause of cancer-related deaths worldwide due to the lack of early diagnostic biomarkers and effective therapeutic targets. Dysregulated ribonucleotide reductase (RNR) expression has been confirmed to be causally linked to tumorigenesis. This study demonstrated that ribonucleotide reductase small subunit M2 (RRM2) is significantly upregulated in ESCC tissue and that its expression is negatively correlated with clinical outcomes. Mechanistically, HuR promotes *RRM2* mRNA stabilization by binding to the adenine/uridine (AU)-rich elements (AREs) within the 3′UTR, resulting in persistent overexpression of RRM2. Furthermore, bifonazole is identified as an inhibitor of HuR *via* computational screening and molecular docking analysis. Bifonazole disrupts HuR-ARE interactions by competitively binding to HuR at F65, R97, I103, and R153 residues, resulting in reduced RRM2 expression.

*Corresponding authors.
E-mail addresses: kdliu@zzu.edu.cn (Kangdong Liu), dongzg@zzu.edu.cn (Zigang Dong).
[†]These authors made equal contributions to this work.
Peer review under the responsibility of Chinese Pharmaceutical Association and Institute of Materia Medica, Chinese Academy of Medical Sciences.

https://doi.org/10.1016/j.apsb.2024.07.022

Cell proliferation

Furthermore, bifonazole exhibited antitumor effects on ESCC patient-derived xenograft (PDX) models by decreasing RRM2 expression and the dNTP pool. In summary, this study reveals the interaction network among HuR, RRM2, and bifonazole and demonstrated that bifonazole is a potential therapeutic compound for ESCC through inhibition of the HuR/RRM2 axis.

1. Introduction

Esophageal squamous cell carcinoma (ESCC) is a digestive system malignancy with a high incidence[1-3]. Given the lack of characteristic early symptoms and effective therapeutic targets, the mortality of ESCC remains high[4-6]. Therefore, revealing the pathogenic mechanism of ESCC and identifying novel therapeutic targets are urgent tasks. Ribonucleotide reductases (RNRs) are a crucial class of rate-limiting enzymes that regulate the biosynthesis of 2′-deoxyribonucleoside 5′-triphosphates, which are essential for DNA synthesis and repair by facilitating dNTP production[7-9]. RNR comprises ribonucleotide reductase regulatory subunit M1 and ribonucleotide reductase small subunit M2 (RRM2)[10,11]. Throughout the cell cycle, RRM2 expression fluctuates to regulate RNR activity, while the expression of ribonucleotide reductase regulatory subunit M1 remains constant.

Notably, RRM2 is frequently overexpressed in various types of cancer cells compared to normal cells, and RRM2 expression is negatively correlated with patient outcomes[12,13]. The upregulation of RRM2 in neoplastic cells facilitates the provision of dNTP for sustaining DNA synthesis and cell proliferation[14]. Furthermore, RRM2 has been demonstrated to positively impact cancer metastasis by regulating the production of thrombospondin-1 and vascular endothelial growth factor[15]. In gastrointestinal cancer, downregulation of RRM2 leads to reduced gemcitabine resistance[16]. Although RRM2 overexpression is significantly associated with chemoresistance and cancer metastasis, the underlying mechanism driving its upregulation in cancers remains poorly elucidated.

HuR belongs to the embryonic lethal abnormal vision protein family and is an RBP known as AU-binding protein[17-19]. It contains three RNA recognition motifs: RNA recognition motifs 1, 2, and 3[20]. RNA recognition motifs 1 and 2 can directly interact with adenine/uridine-rich elements (AREs). RNA recognition motif 3 is involved in the multimerization and assembly of HuR oligomers on target mRNAs[21,22]. The compelling evidence supporting the direct involvement of HuR in tumor progression has sparked considerable interest in developing potent therapeutic inhibitors. Mitoxantrone, 15,16-dihydrotanshinone-1, tanshinone, and tanshinone derivatives can block the interactions between HuR and its target mRNAs[17,23,24]. CMLD2, tanshinone II, suramin, and NSC# 651084 disrupt the binding of HuR to its target mRNAs[25,26]. MS-444, 5-aza-2′-deoxycytidine/trichostatin A can affect HuR translocation[27-29]. Among these inhibitors, suramin, an FDA-approved antitrypanosomal drug, suppresses the progression of oral cancer by binding HuR and inhibiting its function. However, *in vivo* data to support its effectiveness are lacking[17]. In the present study, we investigated the functions of RRM2 in ESCC and revealed the regulatory mechanism underlying RRM2 upregulation in ESCC. Furthermore, we identified bifonazole as an inhibitor of HuR that binds competitively with *RRM2* mRNA to HuR, thereby promoting the decay of *RRM2* mRNA. We also validated bifonazole's antitumor activity *in vivo* using a patient-derived xenograft (PDX) mouse model.

2. Materials and methods

2.1. Chemicals and cell lines

Bifonazole was purchased from Tokyo Chemical Industry Co., Ltd. (TCI, Tokyo, Japan, CAS#60628-96-8). The KYSE150 and KYSE450 cell lines were purchased from the Chinese Academy of Sciences (Shanghai, China) and validated by short tandem repeat profiling. Professor Enmin Li of Shantou University provided the Shantou human embryonic esophageal (SHEE) cell line.

2.2. Animals and diets

Female mice (CB17-SCID) were purchased from Cyagen Biosciences, Inc. (Jiangsu, China). *nu/nu* (nude) mice were purchased from SPF Biotechnology Co., Ltd. (Beijing, China). The mice were housed in a controlled environment with a temperature ranging from 18 to 22 °C and a humidity ranging from 40% to 60% and were provided adequate food and water. The mice were housed in standard cages on a 12 h light−dark cycle. All experimental procedures were approved by Ethics Committee of China-US (Henan) Hormel Cancer Institute (Zhengzhou, Henan, China) and followed the guidelines established by the Institutional Animal Care and Use Committee.

2.3. Western blotting

Western blotting analysis was performed as previously described[30]. Cells were lysed using Beyotime radioimmunoprecipitation assay (RIPA) buffer (Beyotime, Beijing, China, cat# P0013B). The supernatant fractions were harvested. A Solarbio BCA Quantification Kit (Solarbio, Beijing, China, cat# PC0020) was used to measure protein concentrations. After separation by sodium dodecyl sulfate−polyacrylamide gel electrophoresis (SDS−PAGE), the proteins were transferred to polyvinylidene fluoride (PVDF) membranes and incubated overnight with primary antibodies against RRM2 (Abcam, Cambridge, UK, ab57653), HuR (Cell Signaling Technology, Danvers, MA, USA, cat# 12582), Actin (ZSGB-BIO, Beijing, China, cat# TA-09), GAPDH (ZSGB-BIO, Beijing, China, cat# TA-08) and Flag (Sigma, Richmond, BC, Canada, cat# F1804). The membranes were then incubated with secondary antibodies at room temperature for 2 h. The protein bands were visualized using an ImageQuant 800 system (Amersham).

2.4. Quantitative real-time PCR (qPCR) and RNA decay assay

TRIzol (Invitrogen, Carlsbad, CA, USA) was used to extract RNA from cells or tissues. Subsequently, the Takara PrimeScript RT Reagent Kit (Takara, Otsu, Japan, cat# RR047A) was used to reverse transcribe the RNA into cDNA. The mRNA transcript abundance of *RRM2* was quantified using qPCR with a Takara kit (Takara, Otsu, Japan, cat# RR420A). The ΔΔCt method was used to calculate relative RNA abundances, with the *GAPDH* gene serving as an internal control for normalization.

The following primer sequences were used:

RRM2 forward, 5′-CTGGCTCAAGAAACGAGGACTG-3′ and reverse, 5′-CTCTCCTCCGATGGTTTGTGTGTAC-3′.

GAPDH forward, 5′-CAGCCTCAAGATCATCAGCA-3′ and reverse, 5′-TGTGGTCATGAGTCCTTCCA-3′.

KYSE150 and KYSE450 cells were treated with 0.1 μg/mL actinomycin D (0, 2 and 4 h). Subsequently, *RNA* was extracted from ESCC cells using TRIzol reagent, and mRNA levels were analyzed *via* CFX96™ Real-Time System (BIO RAD).

2.5. Luciferase reporter assay

Various fragments of the *RRM2* 3′UTR were inserted into the pmirGLO vector. KYSE150 and KYSE450 cells were seeded into 24-well plates and incubated overnight. The vector (pmirGLO-blank) and pmirGLO-*RRM2* 3′UTR plasmids were transfected separately into ESCC cells. After 24 h, the collected cells were washed 2 times with ice-cold PBS. Subsequently, the cells were lysed at room temperature for 15 min. Following the manufacturer's instructions, an EZ-Magna Dual-Luciferase Reporter Assay Kit (EZ-Magna, Darmstadt, Germany, cat# DL101-01) was used to measure luciferase activity. A microplate reader was used to measure the luciferase fluorescence intensity immediately. Luciferase activity was normalized to the control reporter activity to calculate the relative luciferase activity of the *RRM2* 3′UTR fragments.

2.6. RNA immunoprecipitation (RIP) assay

293T cells were transfected with the pcDNA3.1-3 × Flag-HuR plasmid for 48 h. The cells (1×10^7) were collected and lysed in 1 mL of RIPA buffer. Subsequently, the cell lysates were incubated with antibody-coated beads overnight at 4 °C. The immunoprecipitates were thoroughly washed 5 times with TBST buffer after the supernatant was discarded. The cells in the recovered precipitates were lysed with TRIzol as previously described, and the purified RNA products were then subjected to qPCR analysis to investigate the interactions between HuR and specific target RNAs.

2.7. dNTP pool assay

dNTP levels were measured as previously described[31]. Samples were collected in 550 μL of 60% ice-cold MeOH prior to incubation at 95 °C for 3 min and subsequent cooling on ice. The supernatant fractions were collected after centrifugation at 18,500 × *g* for 6 min at 4 °C and were then transferred to an equilibrated Amicon Ultra 0.5 mL centrifugal filter. Finally, each sample was concentrated, and the residual diethyl ether was evaporated using a Speed-Vac set to a high temperature (65 °C) for 15 min.

2.8. Electrophoretic mobility shift assay (EMSA)

The interaction of HuR with *RRM2* mRNA was detected by EMSA. The EMSA kit was purchased from Thermo Fisher Scientific (Thermo Fisher, Swedesboro, NJ, USA, cat# 20158). The *RRM2*-ARE probe (Supporting Information Fig. S2A) was purchased from GenePharma. Nondenaturing PAGE was performed using a 40% acrylamide gel with 5 × TBE running buffer. The reaction mixture consisted of 4 μg of HuR WT or mutant protein, 1 μL of the ARE probe (125 μmol/L), 5 μL of 5 × loading buffer, 0.2 μL of tRNA, 2 μL of 10 × binding buffer, and 2 μL of 50% glycerol. Electrophoresis was conducted for 60 min at 130 V. The complexes in the gel were then transferred onto a nylon membrane (previously soaked in 0.5 × TBE buffer for at least 10 min) using transfer conditions of 400 mA (∼35 V) for 30 min. After the transfer and drying steps, the membrane was subjected to cross-linking using a 254 nm UV bulb positioned approximately 0.5 cm above the membrane surface for 3−5 min. Finally, biotin-labeled RNA was detected by ImageQuant 800 system (Amersham).

2.9. Surface plasmon resonance (SPR) analysis

SPR analysis was performed with the Biacore T200 instrument (GE Healthcare, Uppsala, Sweden) as previously described[32]. The HuR protein was immobilized on a CM-5 chip (GE Healthcare, Uppsala, Sweden, cat# BR-1005-30), while the *RRM2* mRNA probe was immobilized on an SA chip (GE Healthcare, Uppsala, Sweden, cat# BR-1005-31). The binding affinity between HuR and bifonazole and the interaction between HuR and *RRM2* mRNA were analyzed using T200 evaluation software. The association kinetics, dissociation kinetics, and equilibrium binding constants were determined to characterize the interactions between HuR and the ligands.

2.10. Cellular thermal shift assay (CETSA)

A CETSA was performed following the manufacturer's protocol[33]. 293T cells (1×10^7) were transfected with 10 μg of the WT or mutant HuR plasmid. Following treatment with bifonazole or DMSO for 1 h, the cells were collected in PBS, divided into aliquots of 100 μL each and incubated at different temperatures. After being heated for 3 min, the cells were subjected to two cycles of freezing and thawing. The supernatant fractions were then harvested and quantified for further analysis *via* Western blotting to assess the thermal stability of HuR in the presence of bifonazole or DMSO.

2.11. Animal studies

This study was conducted *via* a protocol approved by Ethics Committee of China-US (Henan) Hormel Cancer Institute (Zhengzhou, Henan, China). Tumor tissues were obtained during surgery from ESCC patients at the Affiliated Cancer Hospital of Zhengzhou University (Zhengzhou, Henan, China) who did not undergo radiotherapy or chemotherapy, and these tissues were implanted into female CB17/SCID mice weighing approximately 20 g. In brief, fresh tumor tissues were fragmented to pieces weighing 0.2 g, which were subcutaneously transplanted into the mice according to a previously described procedure for establishing a PDX mouse model[34]. After one week, when the average tumor volume was approximately 100 mm^3, the mice were

randomly divided into 3 groups: the vehicle group, 50 mg/kg bifonazole group, and 100 mg/kg bifonazole group. Bifonazole was administered by gavage. For the cell-derived xenograft (CDX) model, cells resuspended in cold PBS (1×10^7 cells/100 μL) were injected subcutaneously into each nude mouse. The tumors were measured twice a week, and the tumor volume was calculated using Eq. (1):

$$\text{Volume} = (\text{Length} \times \text{Width} \times \text{Width})/2 \quad (1)$$

When the average tumor volume in the control group was approximately 1000 mm^3, all the mice were sacrificed, and the tumor masses were excised and photographed. Then, the tumor masses were divided into 2 parts: one part was fixed in formalin for hematoxylin and eosin staining and immunohistochemical analysis, and the other part was frozen at −80 °C for protein analysis.

2.12. Immunohistochemical (IHC) analysis

Tissue was fixed in neutral formalin for 72 h and was then dehydrated and embedded in paraffin. Subsequently, the samples were subjected to deparaffinization and rehydration. The tissue sections were then used for standard IHC assays using an anti-RRM2 primary antibody at a 1:200 dilution. Following the immunostaining procedure, the slides were observed and analyzed using TissueGnostics TissueFAXS imaging software (TissueGnostics, Vienna, Austria) to evaluate the expression and localization of RRM2 in the tissue samples. Quantitative analysis of the IHC staining intensity and distribution pattern was performed using an imaging system.

2.13. Study approval

All animal experiments in this study were performed following the Ethics Committee of China-US (Henan) Hormel Cancer Institute (Zhengzhou, Henan, China, CUHCI2022032). Human tumor samples were collected from the Affiliated Cancer Hospital of Zhengzhou University with the permission of the Ethics Committee of Zhengzhou University (Zhengzhou, Henan, China).

2.14. Statistical analysis

All quantitative data are presented as the mean ± standard deviation (SD). One-way ANOVA or Student's t test was performed using SPSS 20 or GraphPad Prism 9.5 software. $P < 0.05$ was considered to indicate statistical significance based on $n \geq 3$ independent experiments ($^*P < 0.05$, $^{**}P < 0.01$, $^{***}P < 0.001$).

2.15. Data availability

The ESCC mRNA expression profile data were obtained from The Cancer Genome Atlas (TCGA) and the Gene Expression Omnibus (GEO) database (GSE44021). The data from this study can be made available upon reasonable request by contacting the corresponding author.

3. Results

3.1. RRM2 is upregulated in ESCC

According to the proteomics results obtained in our multiomics study on ESCC, the protein level of RRM2 was significantly higher ($P < 0.0001$) in ESCC tissues than in adjacent tissues (Fig. 1A). To verify the mRNA expression of *RRM2* in ESCC, we retrieved data from the GEO and TCGA databases. The *RRM2* mRNA level ($P < 0.0001$) was significantly higher in ESCC tissues than in normal tissues (Fig. 1B and Supporting Information Fig. S1A). To further evaluate the protein level of RRM2 in ESCC, we performed IHC staining to evaluate protein expression in a commercial ESCC tissue array. As shown in Fig. 1C, more intense RRM2 staining was observed in tumor tissues than in adjacent tissues. Elevated RRM2 protein levels were detected in both paired ($P < 0.0001$) and unpaired ($P < 0.0001$) ESCC samples (Fig. 1D and E). Western blotting analysis revealed that 83% (10 of 12) of the patient tissue samples exhibited an increased protein level of RRM2 compared to the paired adjacent tissue, as demonstrated in Fig. 1F and Fig. S1B. Moreover, we analyzed the prognostic information from the TCGA database. Clinical correlation analysis revealed that an increased *RRM2* mRNA level was correlated with a shorter overall survival time ($P < 0.0001$) in ESCC patients (Fig. 1G). Collectively, these findings revealed that RRM2 was upregulated in ESCC and that RRM2 upregulation was associated with a poor prognosis.

3.2. RRM2 promotes ESCC cell proliferation in vitro and in vivo

To investigate the function of RRM2 in ESCC, ESCC cells with stable RRM2 silencing were established using two short hairpin RNA (shRNA) sequences. The knockdown efficiency was verified through Western blotting (Fig. 2A). To confirm the direct impact of RRM2 on the proliferation of ESCC cells, MTT and colony formation assays were performed. Notably, RRM2 knockdown dramatically inhibited the proliferation ($P < 0.0001$) and colony formation ($P < 0.0001$) of KYSE150 and KYSE450 cells compared to those in the corresponding mock groups (Fig. 2B−D). RRM2, a major subunit of RNR, plays an indispensable role in DNA synthesis and repair by facilitating the production of dNTP (dATP, dTTP, dCTP, and dGTP)[35]. Therefore, we investigated whether the inhibition of dNTP synthesis could be attributed to RRM2 depletion. Our data revealed a significant decrease in dNTP (dATP, dCTP, dGTP, and dTTP) levels in the RRM2-knockdown cell lines (Fig. 2E). To exclude any potential off-target effects caused by the shRNAs, we restored RRM2 overexpression in RRM2-knockdown cells (Fig. 2F). The impairment of cell proliferation ($P < 0.0001$) and colony formation ($P < 0.0001$) in RRM2-knockdown cells was reversed upon restoration of RRM2 overexpression (Fig. 2G and H). To explore whether RRM2 can promote tumor growth *in vivo*, we established CDX mouse models. Notably, our results demonstrated that the tumor volume ($P < 0.0001$) and tumor weight ($P < 0.0001$) decreased significantly with RRM2 deficiency (Fig. 2I). Collectively, these results elucidate the crucial role of RRM2 in ESCC cell proliferation both *in vitro* and *in vivo*.

3.3. HuR interacts with RRM2 by directly binding to its 3′UTR

To further investigate the mechanism underlying the upregulation of RRM2 in cancer, we analyzed the nucleic acid sequence of *RRM2*. Encouragingly, 12 AREs were predicted in the 3′UTR of *RRM2* mRNA (Fig. S2A). Based on this finding, we speculated that RBPs may be involved in RRM2 upregulation in ESCC. Subsequently, we screened potential *RRM2* mRNA-binding proteins retrieved from the RNA-Binding Protein DataBase (RBPDB). Interestingly, the results suggested that HuR

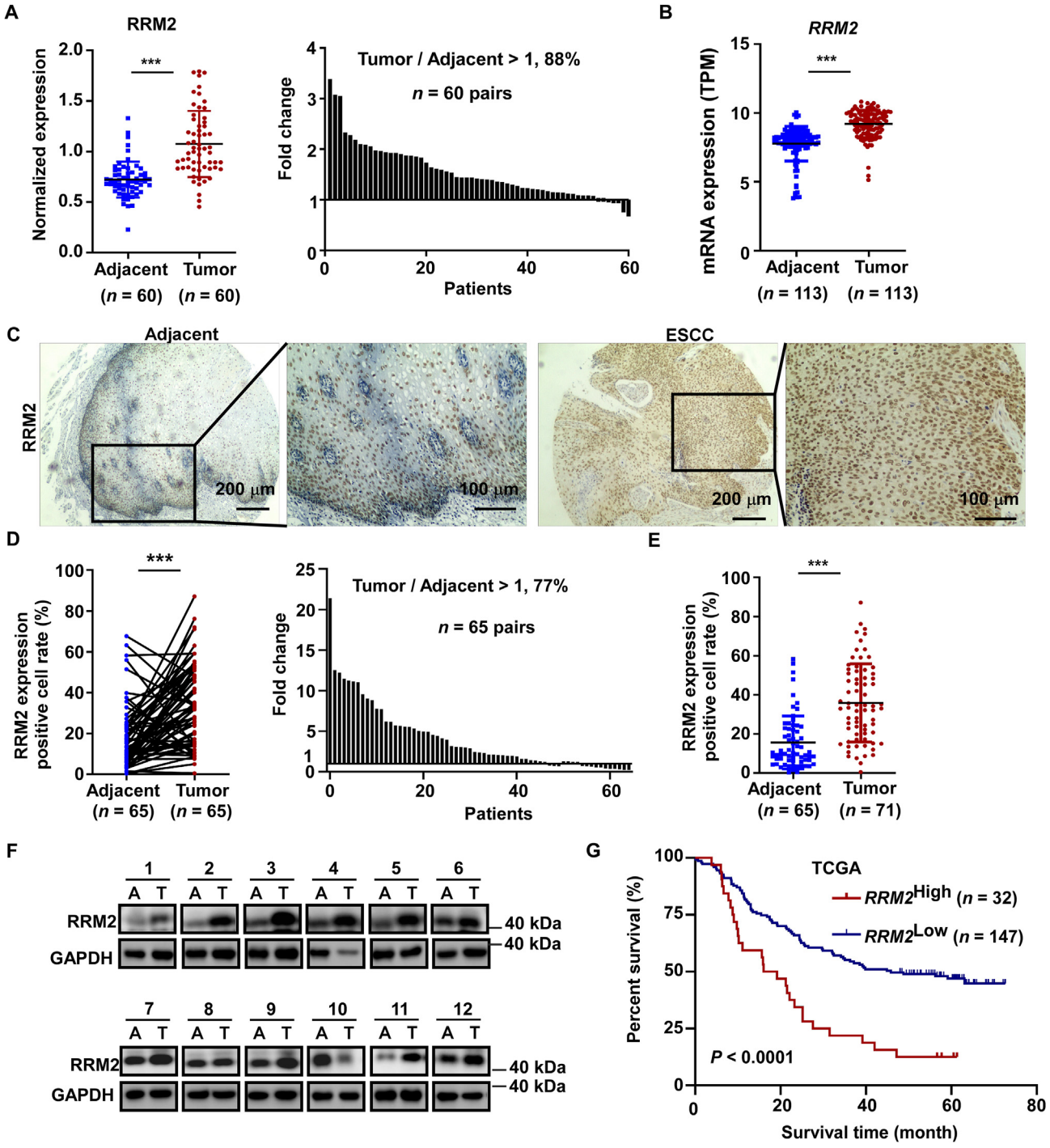

Figure 1 RRM2 is upregulated in ESCC. (A) RRM2 protein levels in ESCC tumor samples compared with adjacent samples (left). Waterfall plot showing the fold changes in RRM2 protein levels in ESCC tumor samples compared with adjacent samples (right), $n = 60$. (B) *RRM2* mRNA levels in ESCC tumor samples compared with adjacent samples in the GEO database (GSE44021), $n = 113$. (C) Representative images of IHC staining in ESCC tumor samples and paired adjacent tissue samples (scale bar: 100 μm; scale bar: 200 μm). (D) RRM2 protein levels in 65 pairs of ESCC tissues (left) and the waterfall plot showing the fold changes in RRM2 protein levels in the 65 pairs of ESCC tissues and adjacent tissues (right), $n = 65$. (E) IHC staining was used to evaluate RRM2 protein expression in microarrays of unpaired ESCC tissues, adjacent = 65, tumor = 71. (F) Protein levels of RRM2 in 12 pairs of ESCC tumor tissues and adjacent tissues, as determined by Western blotting, $n = 12$. (G) Relationship between the *RRM2* mRNA expression level and overall survival in patients represented in the TCGA database. The data are presented as the mean ± SD; $^{*}P < 0.05$; $^{**}P < 0.01$; $^{***}P < 0.001$.

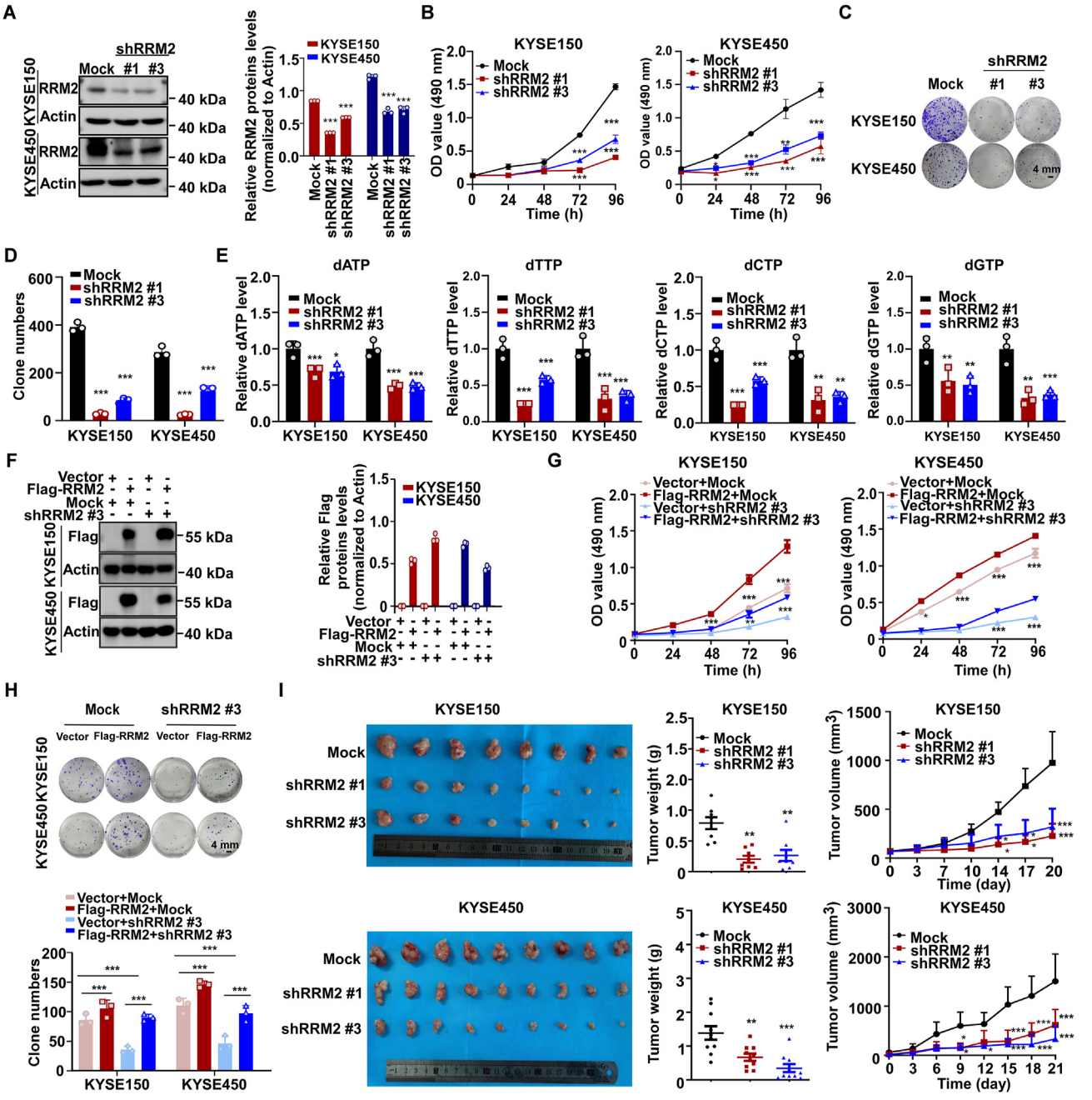

Figure 2 RRM2 overexpression promotes ESCC cell proliferation. (A) Left: Western blotting was used to determine the knockdown efficiency of shRRM2 in ESCC cells. Right: Densitometric analysis of RRM2 protein levels in RRM2-knockdown ESCC cells ($n = 3$). (B) Cell counts for KYSE150 and KYSE450 cells transfected with shRRM2 or mock shRNA. At the 0, 24, 48, 72, and 96 h time points, the cells were treated with MTT solution (0.5 mg/mL), and after 2 h of incubation, the absorbance was measured using a microplate reader. (C, D) Colony formation of KYSE150 and KYSE450 cells after 7 days (scale bar: 4 mm). (E) KYSE150 and KYSE450 cells transfected with shRRM2 or mock shRNA were used for a dNTP pool assay. (F) Left: RRM2 overexpression was restored with the pcDNA3.1-3 × flag-RRM2 plasmid in RRM2-knockdown KYSE150 and KYSE450 cells, and Western blotting was performed to measure the protein level of Flag. Right: Densitometric analysis of RRM2 protein levels in ESCC ($n = 3$). (G) Cell counts for KYSE150 and KYSE450 cells with restoration of RRM2 overexpression. At the 0, 24, 48, 72, and 96 h time points, the cells were treated with MTT solution (0.5 mg/mL), and after 2 h of incubation, DMSO was used to stop the reaction and the absorbance was measured using a microplate reader. (H) Colony formation of KYSE150 and KYSE450 cells after 7 days (scale bar: 4 mm). (I) Orthotopic xenografts were established in nude mice with shRRM2 and control ESCC cells (1×10^7 cells/mouse; KYSE150, 8 mice per group; KYSE450, 9 mice per group). After 20 (KYSE150) and 21 (KYSE450) days, the tumor masses were excised and photographed (left). The tumor weight was calculated (middle). The tumor volume was also calculated, and tumor growth curves were plotted (right). The data are presented as the mean ± SD; $^*P < 0.05$; $^{**}P < 0.01$; $^{***}P < 0.001$.

may be a promising candidate (Fig. S2B). Gene Expression Profiling Interactive Analysis (GEPIA) revealed a positive correlation between the *RRM2* and *HuR* mRNA levels in ESCC (Fig. 3A). Moreover, gene set enrichment analysis (GSEA) revealed that RRM2 and its related genes were upregulated under the condition of high HuR expression (Fig. 3B). Additionally, we analyzed the correlation between the RRM2 and HuR protein levels in 60 pairs of ESCC and adjacent tissues. Among the ESCC tissues with high HuR expression, 57% (17 of 30) had high RRM2 expression, whereas only 43% (13 of 30) had low RRM2 expression (Fig. S2C). Spearman correlation analysis revealed a positive correlation between the HuR and RRM2 protein levels ($R = 0.43$, $P < 0.0001$) in the 60 pairs of clinical ESCC tissues (Fig. 3C). Notably, compared to patients with high levels of both HuR and RRM2 in ESCC tissues, patients with low levels of both HuR and RRM2 tended to have better overall survival (Fig. 3D). Next, we investigated whether HuR can regulate RRM2 expression. The results of qPCR and Western blotting analyses confirmed that HuR knockdown in KYSE150 and KYSE450 cells reduced the *RRM2* mRNA and protein levels (Fig. 3E and F). The results of the dNTP pool assay revealed that HuR knockdown led to decreased dNTP synthesis in ESCC cells (Fig. S2D). These findings indicated that HuR could regulate RRM2 expression in ESCC.

To gain additional insight into the mechanism by which HuR posttranscriptionally controls the stability of *RRM2* mRNA, we evaluated the mRNA stability of RRM2 in HuR knockdown cells. As shown in Fig. 3G, the abundance of remaining *RRM2* mRNA was lower in cells with HuR knockdown than in the corresponding control cells. To explore whether *RRM2* promoter activity is regulated by HuR, a luciferase reporter vector containing the *RRM2* promoter was constructed. The luciferase assay results revealed that the activity of the *RRM2* promoter remained unchanged in ESCC cells following the knockdown of HuR (Fig. 3H, left). To explore the regulatory role of the *RRM2* 3′UTR in RRM2 expression, we constructed a luciferase reporter vector containing the *RRM2* 3′UTR. The results of the luciferase assay indicated decreased luciferase activity in HuR knockdown cells, suggesting that HuR may modulate the expression of RRM2 by binding to the *RRM2* 3′UTR (Fig. 3H, right). A RIP assay was also performed to further confirm that HuR interacts with the *RRM2* transcript. To this end, pcDNA3.1-3 × Flag-HuR was transfected into 293T cells, and the overexpression efficiency was evaluated using Western blotting. The results showed that HuR was successfully overexpressed in 293T cells (Fig. 3I). The subsequent RIP assay results indicated that HuR could bind to *RRM2* mRNA in 293T cells (Fig. 3J). To identify the specific region of HuR that interacts with *RRM2* mRNA, we synthesized biotin-labeled RNA probes for the predicted AREs and performed EMSA (Fig. S2A). The EMSA results showed that HuR could bind to AREs #1 (UUGGCUGAUUUUUUUUUUCC) and #10 (AUCAGAAAUUUUUUAUUAUCUAUGU) (Fig. 3K). We further conducted SPR analysis to compare the affinity of these two AREs for HuR. The affinity of $ARE^{RRM2\#10}$ was higher than that of $ARE^{RRM2\#1}$ (Fig. 3L). Furthermore, several concentrations of $ARE^{RRM2\#10}$ were perfused over immobilized HuR, and $ARE^{RRM2\#10}$ was found to exhibit a dose-dependent affinity for HuR (Fig. 3M, left). Finally, we mutated the U nucleotides in $ARE^{RRM2\#10}$, which are essential for the interaction between HuR and this ARE[36]. The SPR results showed that $ARE^{RRM2\#10MUT}$ could not interact with HuR (Fig. 3M, right). Collectively, our findings demonstrated that HuR might regulate *RRM2* mRNA stability through a functional ARE.

3.4. *HuR promotes ESCC progression by regulating RRM2 expression in ESCC cells*

Subsequently, we investigated the role of HuR in ESCC. The MTT and colony formation assay results demonstrated that HuR knockdown impaired the proliferation and colony formation ability of ESCC cells (Supporting Informaiton Fig. S3A and S3B). Furthermore, proteomic analysis revealed that the HuR protein level was significantly increased ($P < 0.0001$) in tumor tissues (Fig. 4A and B). Kaplan−Meier analysis revealed that ESCC patients with low HuR expression had better overall survival ($P = 0.042$) than did those with high HuR expression (Fig. 4C). Then, the validation of HuR expression was extended to a commercial ESCC tissue array (Fig. S3C). HuR expression was increased in 69 tumor tissues ($P < 0.0001$) compared to the matched normal tissues (Fig. S3D and S3E). We further analyzed a public GEO dataset and found that *HuR* expression was higher in ESCC tissues ($P < 0.0001$) than in normal tissues (Fig. S3F). Furthermore, patients with high HuR expression in ESCC tissues had shorter overall survival times than those with low HuR expression (Fig. S3G). Consistent with these findings, the results of Western blotting analysis revealed that 92% (11 of 12) of the paired ESCC tissues exhibited high protein levels of HuR compared to that in the adjacent tissues (Fig. S3H). These findings prove that HuR is overexpressed in ESCC and that high HuR expression is positively correlated with poor survival in ESCC patients.

Subsequently, we investigated whether RRM2 is an essential downstream target of HuR in ESCC. To this end, we overexpressed RRM2 in HuR knockdown and mock cells (Fig. 4D and Fig. S3I). As expected, RRM2 overexpression reversed the impairment of proliferation and colony formation in HuR knockdown ESCC cells (Fig. 4E and F), indicating that RRM2 is a functional downstream target of HuR. Overall, we confirmed that the HuR-RRM2 axis plays a crucial role in ESCC cell proliferation.

3.5. *Bifonazole inhibits ESCC cell proliferation by downregulating RRM2 expression*

The oncogenic role of the HuR−RRM2 axis prompted us to screen for compounds that might directly target this axis to suppress cancer progression. We performed an *in silico* virtual screen to search for a HuR inhibitor among FDA-approved drugs, and the top 7 candidates are listed in Supporting Information Fig. S4A. Among these drugs, bifonazole, a broad-spectrum antimycotic, exhibited an good inhibitory effect on cell proliferation (Fig. 5A and B). Moreover, bifonazole had minimal impact on the growth of SHEE cells (Fig. 5C). Furthermore, bifonazole inhibited cell proliferation and colony formation in a dose-dependent manner (Fig. 5D and E). Then, to gain a better understanding of the inhibitory mechanism of bifonazole against tumors, proteomic analysis was conducted. A fold change ≤ -1.5 or ≥ 1.5 and $P < 0.05$ were selected as the threshold criteria for significance. Among the 4907 quantifiable proteins, 97 were upregulated and 181 were downregulated (Fig. S4B). The 181 downregulated proteins were involved in 11 signaling pathways, including the p53, progesterone-mediated oocyte maturation, and amino acid biosynthesis pathways (Fig. S4C). Enrichment analysis of the top 10 downregulated pathways revealed significant downregulation of RRM2, CDK1, CDK2, CCNB1, and CCNB2 (Fig. 5F).

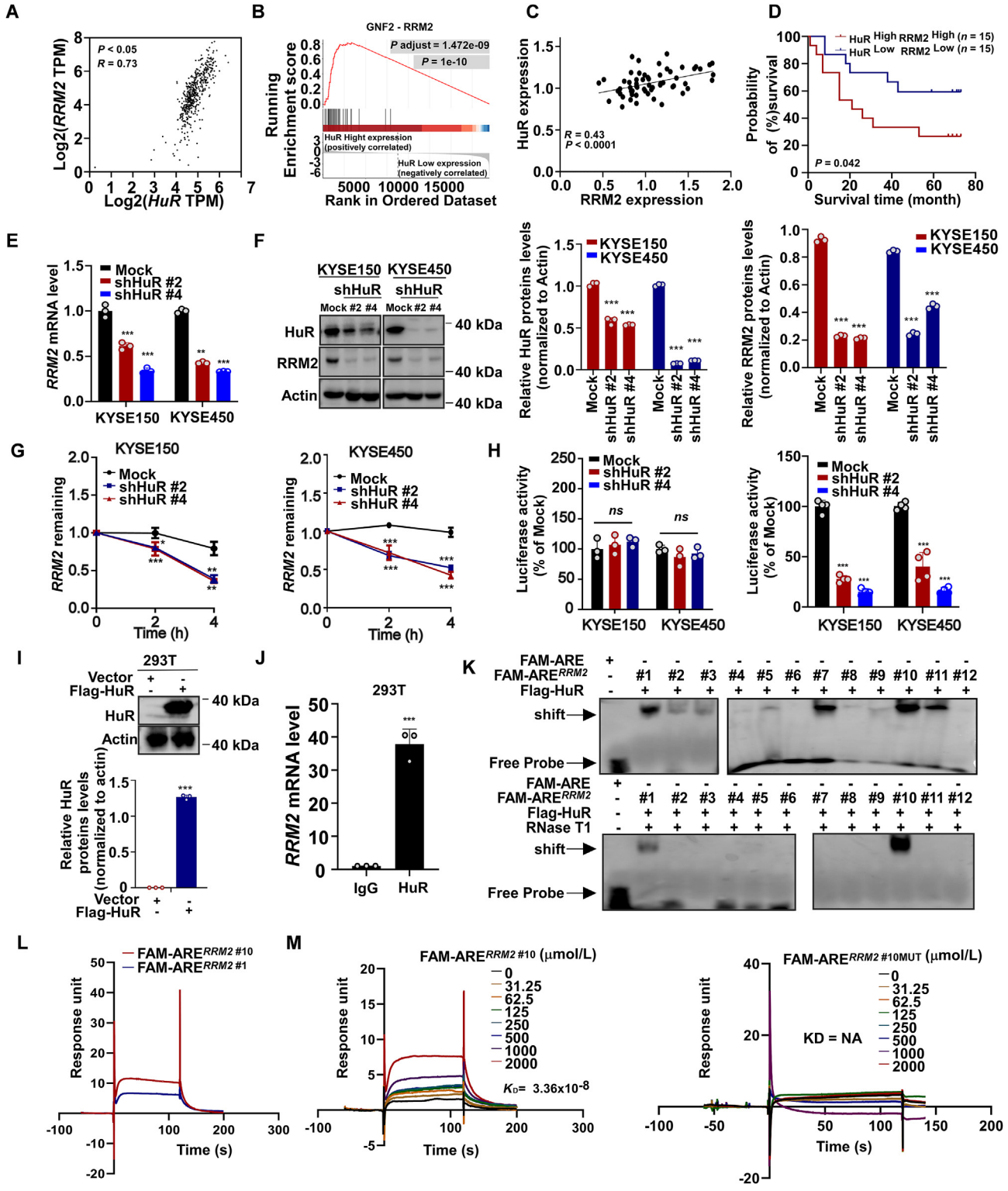

Figure 3 HuR interacts with RRM2 *via* direct binding to the *RRM2* 3′UTR. (A) The correlation between the mRNA levels of *RRM2* and *HuR* was evaluated based on data derived from GEPIA. (B) GSEA was used to explore the expression profiles of genes related to *HuR* expression in TCGA datasets. (C) The association between the protein levels of RRM2 and HuR was investigated in a cohort of 60 paired ESCC tissues. (D) Overall survival analysis was performed to compare survival between the $RRM2^{low}$ and $RRM2^{high}$ groups based on the HuR expression levels in 60 pairs of ESCC tumor samples. (E) qPCR analysis was performed to assess measure the levels of *RRM2* in HuR knockdown KYSE150 and KYSE450 cells. (F) Left: Representative Western blotting results. Right: Densitometric analysis of RRM2 protein levels in HuR knockdown KYSE150 and KYSE450 cells ($n = 3$). (G) Influence of HuR on the mRNA stability of *RRM2* in KYSE150 and KYSE450 cells treated with actinomycin D (0.1 μg/mL). The mRNA abundance was estimated using qPCR. (H) Left: The relative luciferase activity of pGL4.17-RRM2-

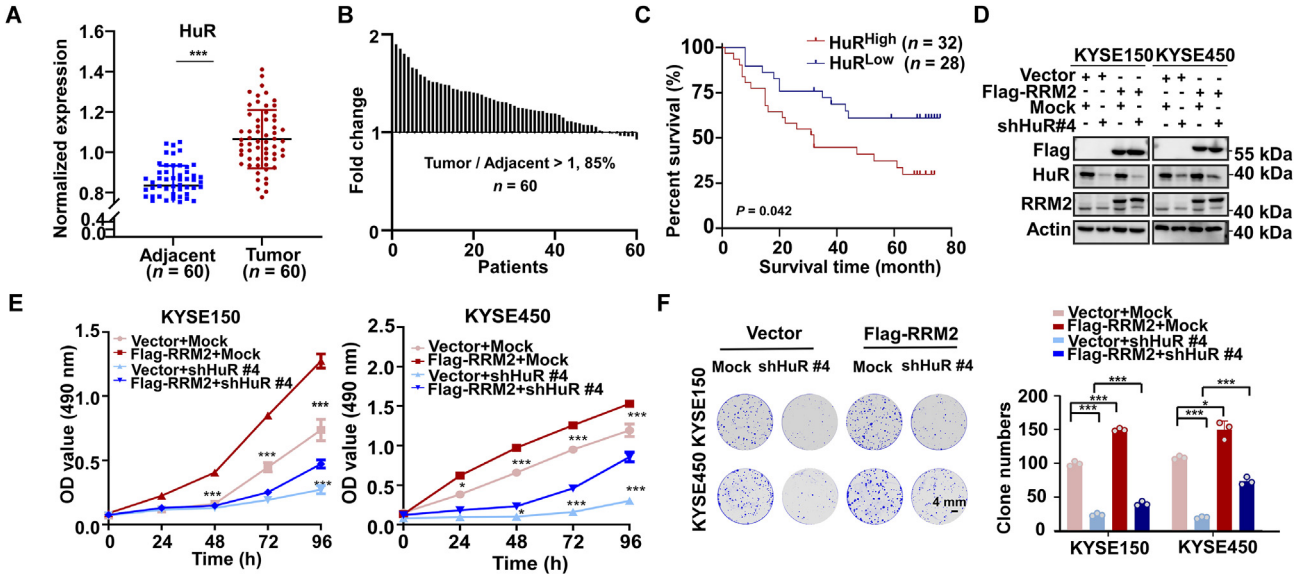

Figure 4 HuR promotes ESCC progression by regulating the expression of RRM2 in ESCC cells. (A) The expression pattern of HuR in 60 pairs of ESCC tumors and their corresponding tissues was determined using proteomic analysis, $n = 60$. (B) A waterfall plot was generated to illustrate the fold change in the expression of HuR in the 60 ESCC clinical samples compared to the paired adjacent tissues, $n = 60$. (C) Kaplan−Meier survival analysis was performed to compare the survival time of ESCC patients between the high HuR expression group and the low HuR expression group. (D) RRM2 overexpression was restored in HuR knockdown KYSE150 and KYSE450 cells, and Western blotting analysis was performed to measure the expression levels of RRM2, Flag, and HuR. (E) Cell counts for KYSE150 and KYSE450 cells transfected with shHuR after restoration of RRM2 overexpression. At the 0, 24, 48, 72, and 96 h, the cells were treated with MTT solution (0.5 mg/mL), and after 2 h of incubation. The absorbance was measured using a microplate reader. (F) Colony formation of HuR knockdown KYSE150 and KYSE450 cells with restoration of RRM2 overexpression after 7 days (scale bar: 4 mm). The data are presented as the mean ± SD; $^{*}P < 0.05$; $^{**}P < 0.01$; $^{***}P < 0.001$.

Notably, RRM2 exhibited the most pronounced downregulation (Fig. 5G). Fig. S4D and S4E show that RRM2 expression was downregulated in ESCC cells after bifonazole treatment. In addition, GSEA result further revealed that RRM2 and its related proteins were significantly downregulated upon bifonazole treatment (Fig. 5H). To confirm whether the synthesis of dNTP decreased after bifonazole treatment, we performed a dNTP pool assay. The results indicated reduced dNTP levels in ESCC cells upon treatment with bifonazole (Fig. 5I). A rescue assay was then conducted to explore the main role of RRM2 in the inhibitory effect of bifonazole on ESCC proliferation. The rescue efficacy was confirmed through Western blotting analysis (Fig. 5J and Fig. S4F). Moreover, to validate the direct influence of RRM2 on the proliferative capacity of ESCC cells treated with bifonazole, MTT and colony formation assays were performed. RRM2 significantly reversed the inhibitory effect of bifonazole on ESCC cell proliferation (Fig. 5K and L). Collectively, these data demonstrated that bifonazole could effectively suppress ESCC cell proliferation by reducing the expression of RRM2.

3.6. *Bifonazole binds to HuR directly*

Molecular docking analysis suggested that bifonazole has the potential to directly interact with HuR. In order to confirm this proposed binding interaction, additional experiments, including Drug Affinity Responsive Target Stability (DARTS), SPR, and CETSA, were carried out. We then performed DARTS and thermal shift assays, and the results showed that bifonazole could bind to HuR (Fig. 6A and B). Additionally, SPR analysis confirmed that bifonazole could bind to the HuR protein in a dose-dependent

Promoter was measured in KYSE150 and KYSE450 cells transfected with shHuR or mock shRNA. Right: The relative luciferase activity of pmirGLO-*RRM2* 3′UTR was measured in KYSE150 and KYSE450 cells transfected with shHuR or mock shRNA. Firefly luciferase activity was measured and normalized to Renilla luciferase activity. (I) Upper: Western blotting was used to determine the overexpression efficiency of HuR in 293T cells. Lower: Densitometric analysis of HuR protein levels in 293T cells ($n = 3$). (J) An anti-HuR antibody was utilized in the RIP assay. After incubation of 293T cells with protein G-agarose beads coated with IgG or the anti-HuR antibody, RNA was extracted from 293T cells. The specific anti-HuR-binding regions in *RRM2* mRNA were identified using qPCR. (K) EMSAs were performed using purified HuR protein, biotin-labeled ARE^{RRM2} probes (125 μmol/L) and 2000 U/mL RNase T1. (L, M) SPR analysis revealed the interaction between HuR and *RRM2* mRNA. ARE^{RRM2} probes (WT or mutant) were fixed on SA chips. The raw response (RU) curves were fitted to a site-specific kinetic model to calculate a K_d value for the interaction. The data are presented as the mean ± SD; $^{*}P < 0.05$; $^{**}P < 0.01$; $^{***}P < 0.001$, "*ns*" indicates no statistically significant difference.

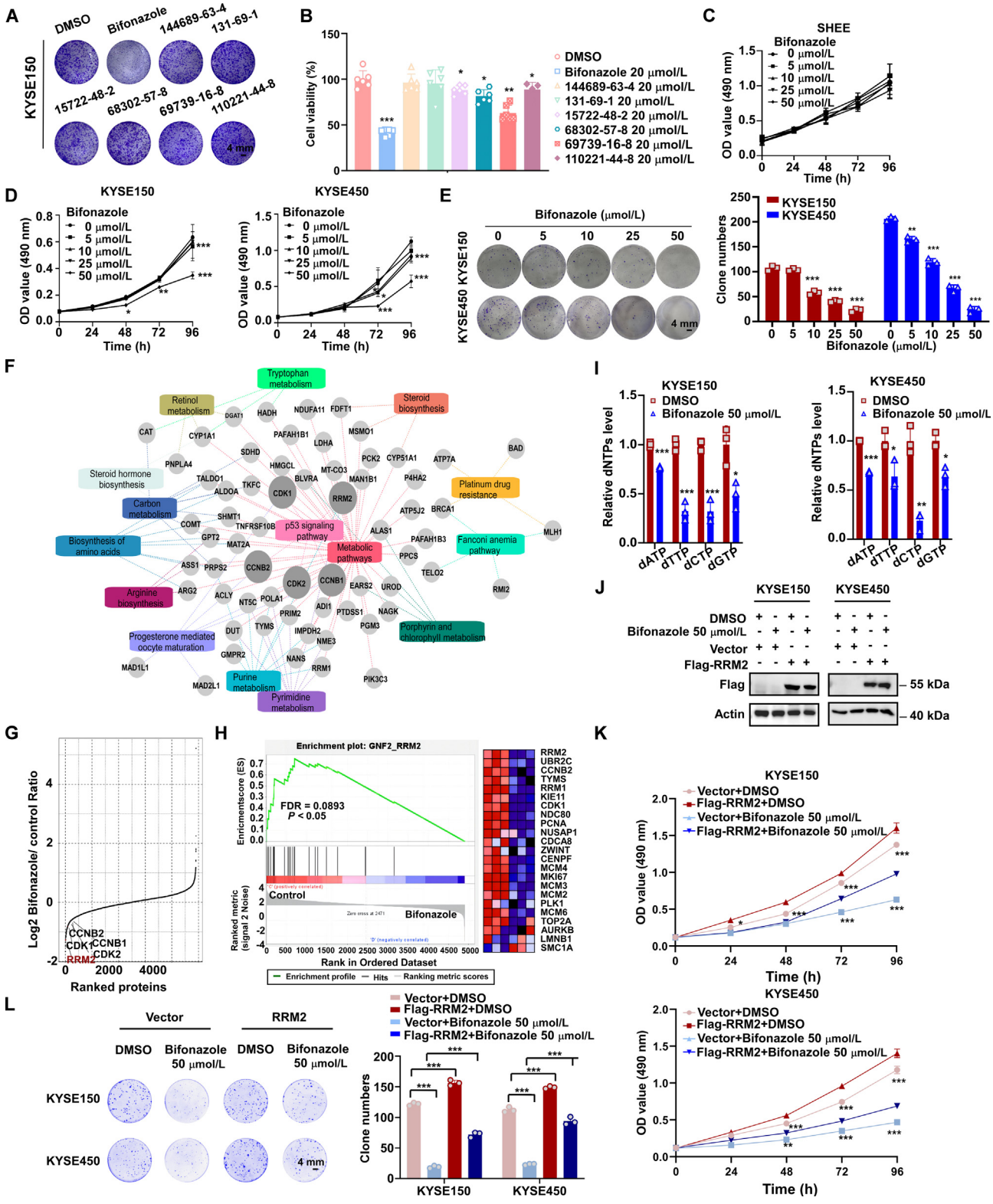

Figure 5 Bifonazole inhibits the proliferation of ESCC cells by regulating the expression of RRM2. (A) A colony formation assay was performed to evaluate the suppressive effects of the top 7 candidate compounds (20 μmol/L) on ESCC cells (scale bar: 4 mm). (B) MTT assays were applied to assess cell viability at 96 h. (C) The normal esophageal cell line SHEE was treated with bifonazole (0, 5, 10, 25, or 50 μmol/L). At the 0, 24, 48, 72, and 96 h, the cells were treated with MTT solution (0.5 mg/mL), and after 2 h of incubation. The absorbance was measured using a microplate reader. (D) KYSE150 and KYSE450 cells were treated with different concentrations of bifonazole for 0, 24, 48, 72, and 96 h. The cells were then treated with MTT solution (0.5 mg/mL), and after 2 h of incubation, the absorbance was measured using a microplate reader. (E) ESCC cells were treated with bifonazole (0, 5, 10, 25, and 50 μmol/L), and colonies were stained with 3% crystal violet after treatment for 12

manner (Fig. 6C). The inhibitory effect of bifonazole on cell proliferation was decreased in HuR knockdown cells, indicating the crucial role of HuR as the target of bifonazole (Fig. 6D). Then, a molecular docking study was performed to determine the potential binding mode of bifonazole with HuR. As shown in Fig. 6E, bifonazole interacts with HuR at residues F65, R97, I103, and R153, which are located in the cleft formed by two RNA recognition domains. Bifonazole forms a hydrogen bond with the backbone of R97, while its dual phenyl groups participate in cation−π interactions with both R97 and R153. In addition, hydrophobic interactions are established between bifonazole and F65 as well as I103. To further determine whether these residues of HuR contribute to its interaction with bifonazole, we mutated each of these residues individually (Fig. 6F). The CETSA and SPR analysis results indicated weakened interactions between bifonazole and the mutated HuR proteins (Fig. 6G and H, Supporting Information Fig. S5). These data confirm that bifonazole can bind to HuR directly.

3.7. *Bifonazole binds competitively with ARE^{RRM2} to HuR*

Subsequently, we investigated the mechanism by which bifonazole regulates RRM2 expression *via* HuR. As RNA binding motifs 1 and 2 are the main ARE-binding domains in the HuR protein, we simulated the binding mode of *RRM2* mRNA with HuR. Molecular docking analysis (Fig. 7A) revealed a compelling interaction wherein a U-rich motif within *RRM2* mRNA binds to HuR at the same site as bifonazole. Specifically, the phosphate group of U13 forms an electrostatic interaction with the side chains of R153, while U14 establishes a hydrogen bond with the side chains of R97. Additionally, the base of A15 participates in $\pi-\pi$ stacking interactions with the side chains of F65. The EMSA and SPR analysis results confirmed that the HuR F65A, R97A, I103A, and R153A mutants exhibited significantly attenuated interactions with ARE$^{RRM2\#10}$ (Fig. 7B and C). To gain a deeper understanding of the importance of ARE$^{RRM2\#10}$, a mutant probe for ARE$^{RRM2\#10MUT}$ was synthesized. ARE$^{RRM2\#10MUT}$ could not bind to WT HuR or the HuR mutants (Fig. 7D). Considering the crucial involvement of residues F65, R97, I103, and R153 in the interaction between HuR and bifonazole, it can be inferred that bifonazole may compete with *RRM2* mRNA for binding to HuR. RIP assays revealed that bifonazole blocked the binding of HuR to the *RRM2* 3′UTR (Fig. 7E and F). Luciferase reporter assays showed that the activity of firefly luciferase (with RRM2 promoter) remained unchanged in ESCC cells after bifonazole treatment (Supporting Information Fig. S6). However, the activity of firefly luciferase (with an ARE sequence at the 3′UTR) was dramatically decreased in response to bifonazole treatment in a concentration-dependent manner (Fig. 7G). Moreover, bifonazole attenuated the interaction between HuR and *RRM2* mRNA in a dose-dependent manner (Fig. 7H). These results confirmed that bifonazole and *RRM2* mRNA could competitively bind to HuR. Subsequently, we investigated whether bifonazole can disrupt *RRM2* mRNA stability. Bifonazole significantly promoted the degradation of *RRM2* mRNA (Fig. 7I). In summary, we conclude that bifonazole accelerates *RRM2* mRNA degradation by disrupting the HuR-ARE interaction.

3.8. *Bifonazole exhibits antitumor effects in vivo*

To investigate the antitumor effects of bifonazole *in vivo*, we established two ESCC PDX models with HuR high expression (Fig. 8A). After oral gavage with bifonazole, the tumor volumes and weights were calculated. The results indicated that bifonazole significantly retarded tumor growth in the bifonazole treatment group compared to the control group (Fig. 8B). Furthermore, to determine whether the antitumor effect of bifonazole is associated with the HuR−RRM2 axis, the RRM2 protein levels were measured in tumor tissues from mice in each group. IHC analysis revealed that the protein level of RRM2 was decreased after bifonazole treatment in the LEG388 and LEG397 tumors (Fig. 8C). We also detected a notable reduction in dNTP levels in tumors from mice in the bifonazole treatment group (Fig. 8D). Together, these results support the conclusion that bifonazole inhibits tumor growth and downregulates RRM2 *in vivo*.

4. Discussion

Abnormal dNTP levels increase genomic instability by regulating DNA replication[12,37]. RRM2 plays an essential role in regulating the levels of dNTP pools, ensuring that their balance is maintained[38]. Multiple studies have shown that RRM2 acts as an oncogene in multiple cancers[39-41]. RRM2 is overexpressed in resistant esophageal cancer cells and tissues after chemoradiotherapy[42,43]. However, the function and transcriptional regulatory mechanism of RRM2 in ESCC are still unclear. In this study, we confirmed the function of RRM2 in promoting cell proliferation and tumor growth by affecting dNTP synthesis. Additionally, ESCC patients with increased RRM2 expression had a poor prognosis. This discovery will improve our understanding of the mechanism underlying RRM2 overexpression.

RBPs are essential for controlling mRNA stability and translation posttranscriptionally[44-46]. RBPs regulate mRNA expression primarily by binding to various RNA regulatory elements, including the AREs in both 3′ and 5′ UTRs[47,48]. FXR1 stabilizes *C-MYC* expression by binding to its ARE in ovarian cancer cells[49]. In breast cancer, RBMS2 stabilizes *P21* mRNA by binding to the ARE in its 3′UTR, inhibiting cancer cell proliferation[50].

days. (F) Proteomic analysis was performed to identify the differentially expressed proteins between the control (DMSO) and bifonazole (50 μmol/L) groups. We focused mainly on the proteins with enrichment in the downregulated pathways. The size of each point represents the degree of differential expression. (G) Rankings of RRM2, CDK1, CDK2, CCNB1, and CCNB2 in the quantitative complete proteome according to the Log2 fold change in their expression between the DMSO- and bifonazole-treated groups. (H) GSEA showed the enrichment of RRM2-related proteins after bifonazole treatment. (I) ESCC cells treated with bifonazole (50 μmol/L) were used for a dNTP pool assay. Paired Student's *t* test was used for statistical analysis. (J) RRM2 overexpression was restored in KYSE150 and KYSE450 cells prior to treatment with bifonazole (50 μmol/L), and Western blotting analysis was performed to measure the Flag expression level ($n = 3$). (K, L) Cell proliferation and colony formation assays were performed in KYSE150 and KYSE450 cells treated with bifonazole (50 μmol/L) after restoration of RRM2 overexpression (scale bar: 4 mm). The data are presented as the mean ± SD; *$P < 0.05$; **$P < 0.01$; ***$P < 0.001$.

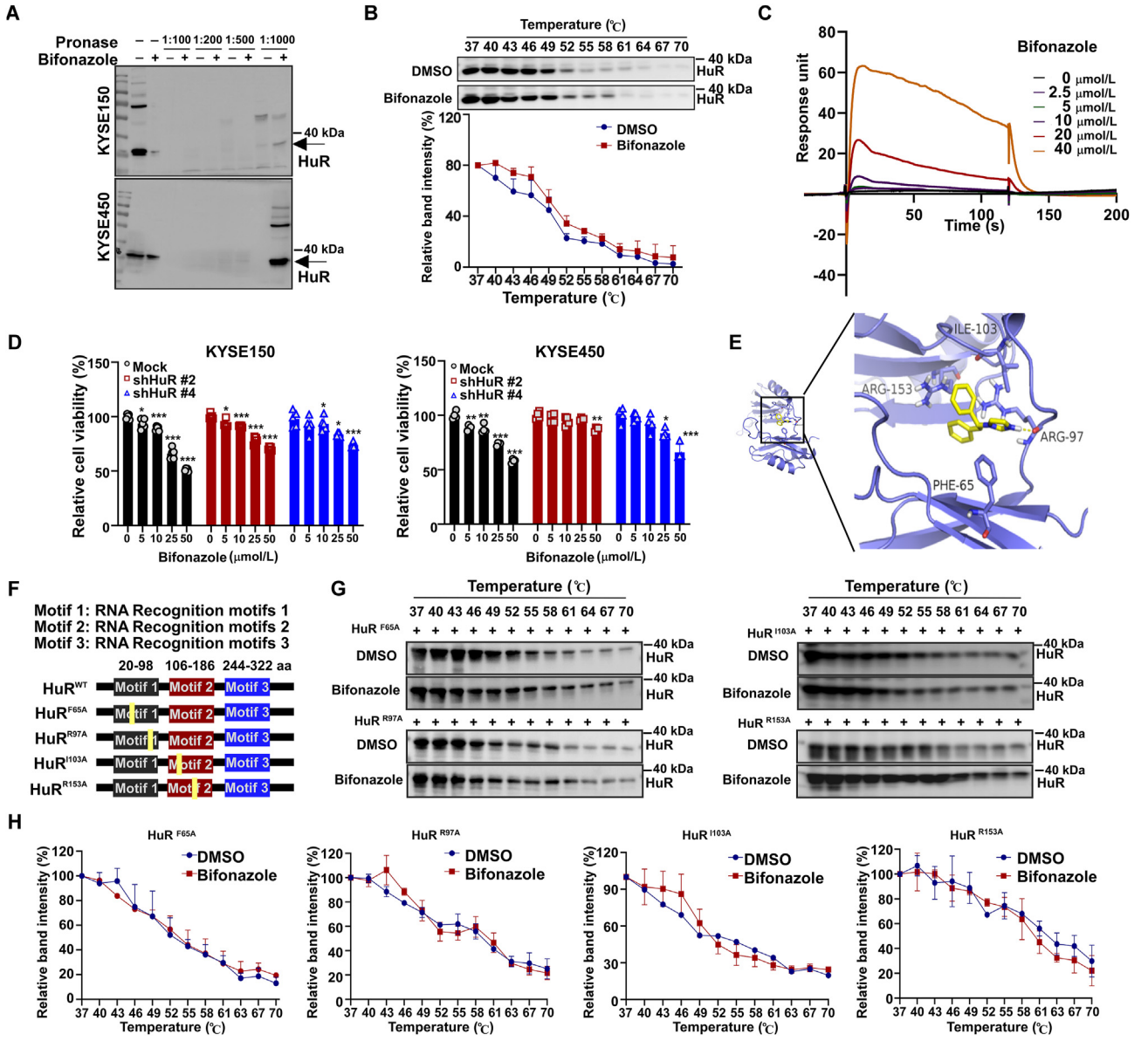

Figure 6 Bifonazole directly targets HuR. (A) The change in the binding intensity between bifonazole and HuR after pronase treatment was assessed. (B) Upper: Western blotting was performed to analyze the results of the CETSA. Lower: relative band intensity of HuR in the control and bifonazole (50 μmol/L) treatment groups. (C) SPR analysis was conducted to examine the interaction between bifonazole and HuR. The raw response (RU) curves were fitted to a site-specific kinetic model to calculate a Kd value for the interaction. (D) HuR knockdown and mock shRNA-transfected KYSE150 and KYSE450 cells were treated with bifonazole (0, 5, 10, 25, and 50 μmol/L), and cell viability was analyzed at 48 h. (E) The crucial amino acids involved in the interaction between HuR and bifonazole were identified by *in silico* docking analysis. (F) The diagram shows different HuR mutation sites. (G) The binding between HuR mutant proteins and bifonazole was examined using Western blotting analysis and CETSA. (H) Relative band intensities of HuR mutant proteins in the control and bifonazole treatment groups. The data are presented as the mean ± SD; $^{*}P < 0.05$; $^{**}P < 0.01$; $^{***}P < 0.001$.

Here, we revealed that the RBP HuR increased *RRM2* mRNA stability by binding to its 3′UTR. Furthermore, the SPR analysis and EMSA results demonstrated that HuR could not bind to *RRM2* after one UUUU sequence within the *RRM2* 3′UTR was mutated. Thus, we revealed the molecular mechanisms underlying RRM2 overexpression in ESCC. In addition, the expression of RRM2 at both the transcriptional and translational levels was found to be regulated by HuR both *in vitro* and *in vivo*. The rescue assay results demonstrated that when RRM2 was overexpressed in HuR knockdown cells, the cell proliferation ability was restored both *in vivo* and *in vitro*. Therefore, we discovered a novel regulatory relationship between HuR and RRM2 in ESCC. These data may contribute to the development of an effective therapeutic strategy for ESCC *via* posttranscriptional targeting.

Currently, the treatment of ESCC is limited due to the lack of effective therapeutic targets and drugs[51,52]. Several attempts have been made to identify small molecule compounds that target RBPs and interfere with RNA binding to provide new cancer treatment

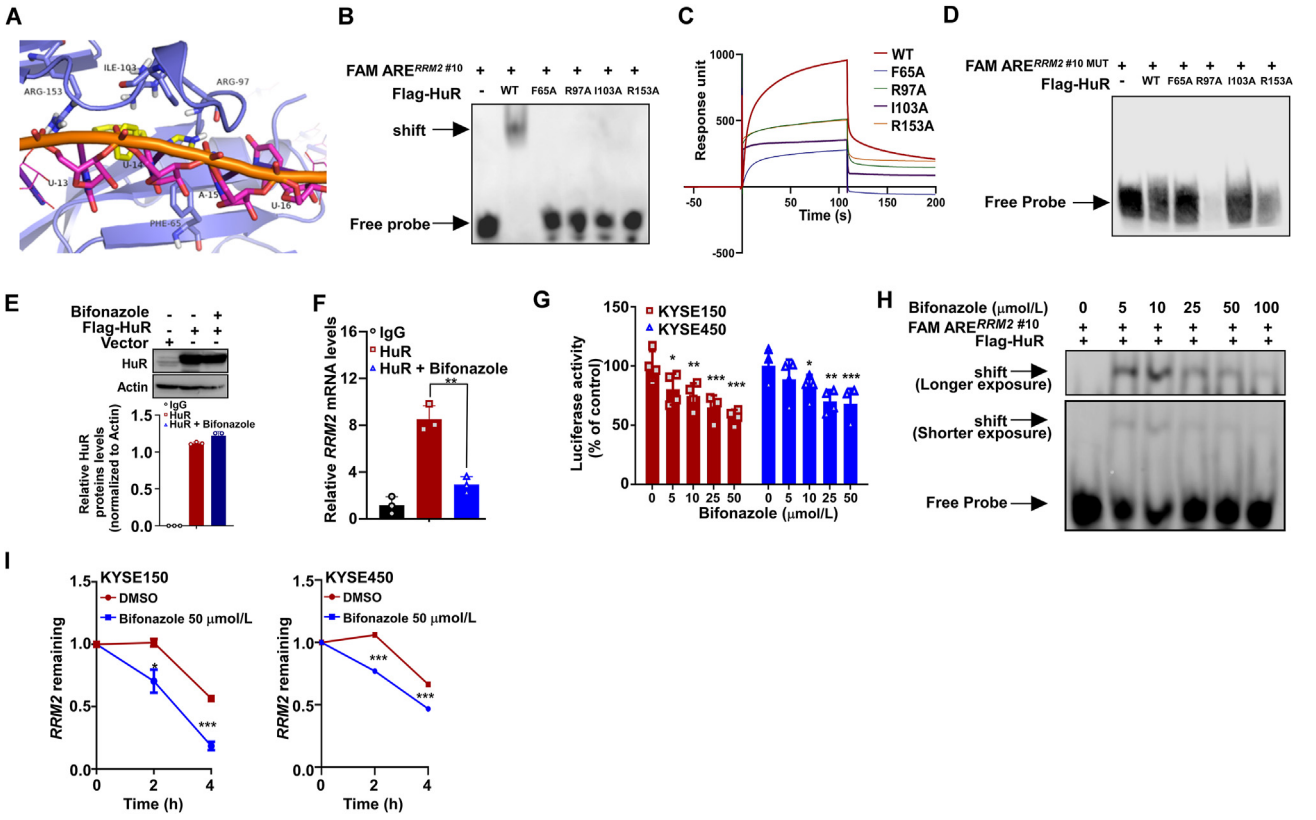

Figure 7 Bifonazole binds competitively with ARE^{RRM2} to HuR. (A) Diagram showing the selected key amino acids involved in the interactions of bifonazole (yellow) and ARE^{RRM2} (orange) with HuR (purple). (B) EMSA was performed with 3′-biotin-labeled ARE^{RRM2} probes and purified HuR (WT or mutant) protein. The concentration of the biotinylated probe was 2 μg/mL. (C) SPR analysis of the interactions between HuR (WT or mutant) and the biotin-labeled ARE^{RRM2} probes. The raw response (RU) curves were fitted to a site-specific kinetic model to calculate a K_d value for the interaction. (D) EMSA was performed with 3′-biotin-labeled ARE$^{RRM2\#10MUT}$ and purified HuR WT protein. The concentration of the biotinylated probe was 125 μmol/L. (E) Upper: Western blotting was used to determine the overexpression efficiency of HuR in 293T cells (treated with bifonazole or left untreated). Lower: Densitometric analysis of the HuR protein level in 293T cells ($n = 3$). (F) An anti-HuR antibody was utilized in the RIP assay. After incubation of 293T cells with protein G-agarose beads coated with IgG or the anti-HuR antibody, RNA was extracted. The specific anti-HuR-binding regions in *RRM2* mRNA were identified using qPCR. The concentration of bifonazole was 50 μmol/L, and the treatment time was 24 h. (G) Relative luciferase activity of pmirGLO-*RRM2* 3′UTR in ESCC cells treated with either 50 μmol/L bifonazole or DMSO. The activity of firefly luciferase was measured and then normalized to the activity of *Renilla* luciferase. (H) EMSA was performed to analyze the interaction between HuR and *RRM2* in the presence of bifonazole (0, 5, 10, 25, and 50 μmol/L). The mixture was incubated for 15 min. (I) qPCR was performed to estimate the impact of bifonazole on *RRM2* mRNA stability in ESCC cells treated with actinomycin D (0.1 μg/mL). The data are presented as the mean ± SD; $^*P < 0.05$; $^{**}P < 0.01$; $^{***}P < 0.001$.

options[53-55]. In the present study, we identified bifonazole, which targets the RNA-binding motifs of HuR, by integrating a drug repurposing strategy and molecular docking simulation. The known HuR inhibitors, such as CLMD2, suramin, and tanshinone II, primarily disrupt the binding of HuR to RNA. In addition to this mechanism, both MS-444 and 5-aza-2′-deoxycytidine/trichostatin A directly interfere with the translocation of HuR, thereby providing an additional mode of HuR inhibition[17]. However, these HuR inhibitors have not been applied successfully in clinical practice. Here, we demonstrated that bifonazole disrupted the interaction between HuR and the ARE^{RRM2}, inhibiting ESCC tumor growth without affecting mouse body weight. More importantly, we revealed that amino acids R153, I103, R97, and F65 are the crucial binding sites in HuR and interact with both *RRM2* mRNA and bifonazole.

According to our proteomics data, the expression of UBE2C and CCNB1 was downregulated at the translational level (Supporting Information Fig. S7). Both *UBE2C* and *CCNB1* are known target mRNAs of *HuR*. This finding suggests that *RRM2* is not the sole target mRNA of HuR in ESCC. However, the rescue assay data demonstrated that overexpression of RRM2 significantly reversed the inhibition of cell proliferation caused by silencing HuR. Therefore, we conclude that while RRM2 is not the exclusive downstream target of HuR, it still plays a crucial role in the oncogenic effect of HuR. Overall, our findings demonstrate that the HuR−RRM2 axis is essential for ESCC growth and

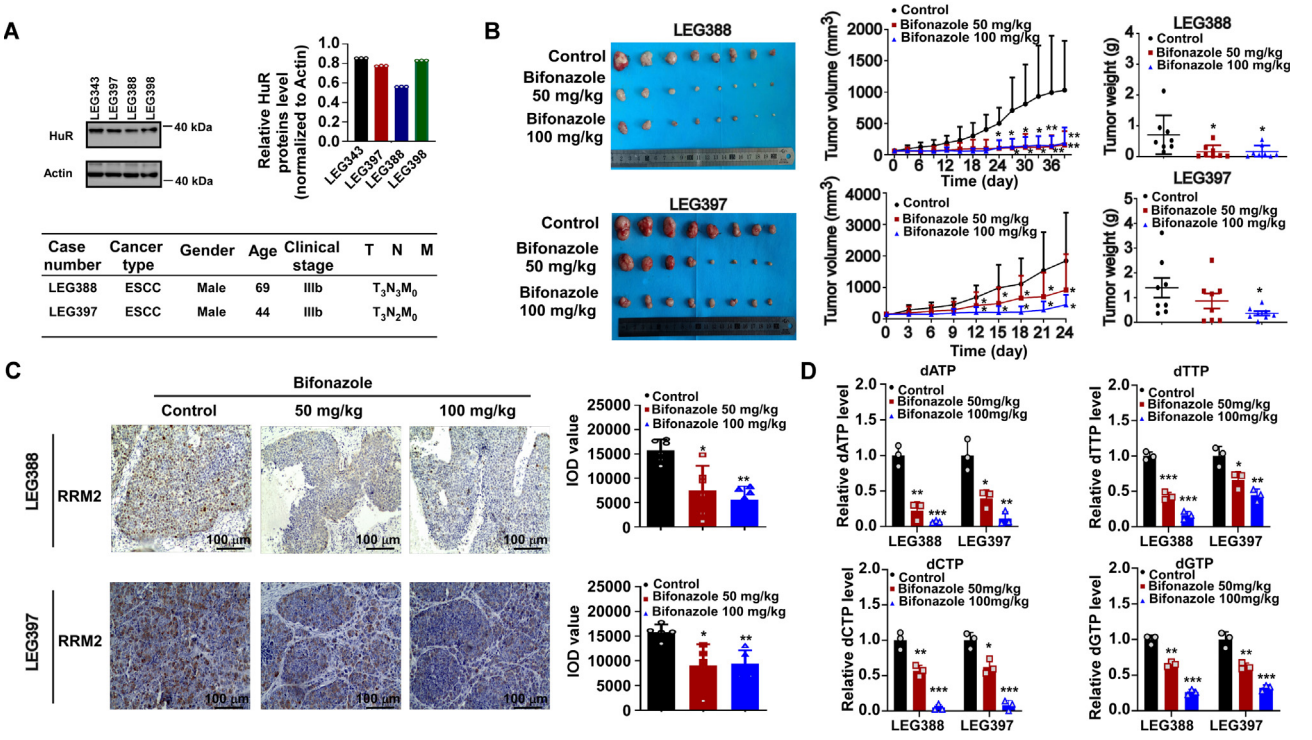

Case number	Cancer type	Gender	Age	Clinical stage	T	N	M
LEG388	ESCC	Male	69	IIIb	T_3	N_3	M_0
LEG397	ESCC	Male	44	IIIb	T_3	N_2	M_0

Figure 8 Bifonazole exhibits antitumor effects *in vivo*. (A) Protein levels of HuR in different PDX tumors (left). Densitometric analysis of HuR protein levels in ESCC tissues ($n = 3$) (right). Clinical information corresponding to two PDXs (lower). (B) Mice were treated with bifonazole (50 mg/kg, 100 mg/kg) or sterile water. After 36 or 24 days, the tumor masses were excised and photographed (left). The tumor volume and growth curves were generated (middle). The tumor weight was measured (right), $n = 8$. (C) Representative images of IHC staining for RRM2 in LEG388 and LEG397 tumor tissues (50 × magnification) after DAB staining. Scale bar, 100 μm (left). The number of positive cells was calculated using the Image-Pro Plus software program (right), $n = 3$. (D) Tissues from the LEG388 and LEG397 tumors from mice treated with bifonazole were used for a dNTP pool assay, $n = 3$. The data are presented as the mean ± SD; $^*P < 0.05$; $^{**}P < 0.01$; $^{***}P < 0.001$.

emphasize the potential applicability of bifonazole for ESCC therapy.

5. Conclusions

Our findings elucidate the oncogenic role of RRM2 in promoting ESCC cell proliferation by increasing *RRM2* mRNA stability through HuR-mediated mechanisms. Furthermore, we identify bifonazole as a potent inhibitor of ESCC tumor growth through competitive binding to HuR. Our findings thus highlight the therapeutic potential of targeting the HuR−RRM2 axis in ESCC.

Acknowledgments

This work was funded by National Natural Science Foundation of China (grant numbers: 81872335, 82303891 and 82303119), The Central Plains Science and Technology Innovation Leading Talents (No. 224200510015, China), Key scientific research project plan of colleges and universities in Henan Province (grant number: 24A310025, China), Science and Technology Project of Henan Province (No. 242102310414, China).

Author contributions

Jing Zhang designed and performed most of the assays. Qiong Wu assisted with the design of the study and analyzed data. Yifei Xie, Huifang Wei, and Yanan Jiang prepared and revised the manuscript. Feng Li, Yinhua Li, and Dengyun Zhao conceived the study. Yan Qiao conducted the computer docking model. Yanan Sun, Han Huang, and Mengmeng Ge helped in animal experiments. Zigang Dong and Kangdong Liu conceived and supervised the study. All authors critically revised the manuscript and approved the final manuscript.

Conflicts of interest

The authors declare no conflict of interests.

Appendix A. Supporting information

Supporting information to this article can be found online at https://doi.org/10.1016/j.apsb.2024.07.022.

References

1. Zhang GC, Yu XN, Guo HY, Sun JL, Liu ZY, Zhu JM, et al. PRP19 enhances esophageal squamous cell carcinoma progression by reprogramming SREBF1-dependent fatty acid metabolism. *Cancer Res* 2023;**83**:521−37.
2. Chen L, Zhang W, Chen D, Yang Q, Sun S, Dai Z, et al. RBM4 dictates ESCC cell fate switch from cellular senescence to glutamine-addiction survival through inhibiting LKB1−AMPK−axis. *Signal Transduct Target Ther* 2023;**8**:159.
3. He S, Xu J, Liu X, Zhen Y. Advances and challenges in the treatment of esophageal cancer. *Acta Pharm Sin B* 2021;**11**:3379−92.

4. Yang YM, Hong P, Xu WW, He QY, Li B. Advances in targeted therapy for esophageal cancer. *Signal Transduct Target Ther* 2020;**5**:229.
5. Wei Y, Wu W, Jiang Y, Zhou H, Yu Y, Zhao L, et al. Nuplazid suppresses esophageal squamous cell carcinoma growth *in vitro* and *in vivo* by targeting pak4. *Br J Cancer* 2022;**126**:1037−46.
6. Zheng C, Yu X, Liang Y, Zhu Y, He Y, Liao L, et al. Targeting PFKl with penfluridol inhibits glycolysis and suppresses esophageal cancer tumorigenesis in an AMPK/FOXO3a/BIM-dependent manner. *Acta Pharm Sin B* 2022;**12**:1271−87.
7. Zuo Z, Zhou Z, Chang Y, Liu Y, Shen Y, Li Q, et al. Ribonucleotide reductase M2 (RRM2): regulation, function and targeting strategy in human cancer. *Genes Dis* 2024;**11**:218−33.
8. Yang PM, Lin LS, Liu TP. Sorafenib inhibits ribonucleotide reductase regulatory subunit M2 (RRM2) in hepatocellular carcinoma cells. *Biomolecules* 2020;**10**:117.
9. Chen Y, Shao X, Cao J, Zhu H, Yang B, He Q, et al. Phosphorylation regulates cullin-based ubiquitination in tumorigenesis. *Acta Pharm Sin B* 2021;**11**:309−21.
10. Gautam A, Bepler G. Suppression of lung tumor formation by the regulatory subunit of ribonucleotide reductase. *Cancer Res* 2006;**66**:6497−502.
11. Xiong W, Zhang B, Yu H, Zhu L, Yi L, Jin X. RRM2 regulates sensitivity to sunitinib and PD-1 blockade in renal cancer by stabilizing anxa1 and activating the Akt pathway. *Adv Sci* 2021;**8**:e2100881.
12. Mazzu YZ, Armenia J, Chakraborty G, Yoshikawa Y, Coggins SA, Nandakumar S, et al. A novel mechanism driving poor-prognosis prostate cancer: overexpression of the dna repair gene, ribonucleotide reductase small subunit M2 (RRM2). *Clin Cancer Res* 2019;**25**:4480−92.
13. Nunes C, Depestel L, Mus L, Keller KM, Delhaye L, Louwagie A, et al. RRM2 enhances MYCN-driven neuroblastoma formation and acts as a synergistic target with CHK1 inhibition. *Sci Adv* 2022;**8**:eabn1382.
14. Chen CW, Li Y, Hu S, Zhou W, Meng Y, Li Z, et al. DHS (*trans*-4,4′-dihydroxystilbene) suppresses DNA replication and tumor growth by inhibiting RRM2 (ribonucleotide reductase regulatory subunit M2). *Oncogene* 2019;**38**:2364−79.
15. Zhang K, Hu S, Wu J, Chen L, Lu J, Wang X, et al. Overexpression of RRM2 decreases thrombspondin-1 and increases VEGF production in human cancer cells *in vitro* and *in vivo*: implication of RRM2 in angiogenesis. *Mol Cancer* 2009;**8**:11.
16. Jung CP, Motwani MV, Schwartz GK. Flavopiridol increases sensitization to gemcitabine in human gastrointestinal cancer cell lines and correlates with down-regulation of ribonucleotide reductase M2 subunit. *Clin Cancer Res* 2001;**7**:2527−36.
17. Majumder M, Chakraborty P, Mohan S, Mehrotra S, Palanisamy V. HuR as a molecular target for cancer therapeutics and immune-related disorders. *Adv Drug Deliv Rev* 2022;**188**:114442.
18. Schultz CW, Preet R, Dhir T, Dixon DA, Brody JR. Understanding and targeting the disease-related rna binding protein human antigen R (HuR). *Wiley Interdiscip Rev RNA* 2020;**11**:e1581.
19. Zhu Y, Yang L, Xu J, Yang X, Luan P, Cui Q, et al. Discovery of the anti-angiogenesis effect of eltrombopag in breast cancer through targeting of HuR protein. *Acta Pharm Sin B* 2020;**10**:1414−25.
20. Zhang W, Pan X, Xu Y, Guo H, Zheng M, Chen X, et al. Mevalonate improves anti-PD-1/PD-L1 efficacy by stabilizing CD274 mRNA. *Acta Pharm Sin B* 2023;**13**:2585−600.
21. Simone LE, Keene JD. Mechanisms coordinating ELAV/Hu mRNA regulons. *Curr Opin Genet Dev* 2013;**23**:35−43.
22. Hinman MN, Lou H. Diverse molecular functions of Hu proteins. *Cell Mol Life Sci* 2008;**65**:3168−81.
23. D'Agostino VG, Adami V, Provenzani A. A novel high throughput biochemical assay to evaluate the hur protein−RNA complex formation. *PLoS One* 2013;**8**:e72426.
24. Manzoni L, Zucal C, Maio DD, D'Agostino VG, Thongon N, Bonomo I, et al. Interfering with HuR−RNA interaction: design, synthesis and biological characterization of tanshinone mimics as novel, effective hur inhibitors. *J Med Chem* 2018;**61**:1483−98.
25. Allegri L, Baldan F, Roy S, Aube J, Russo D, Filetti S, et al. The HuR CMLD-2 inhibitor exhibits antitumor effects *via* MAD2 down-regulation in thyroid cancer cells. *Sci Rep* 2019;**9**:7374.
26. Kakuguchi W, Nomura T, Kitamura T, Otsuguro S, Matsushita K, Sakaitani M, et al. Suramin, screened from an approved drug library, inhibits hur functions and attenuates malignant phenotype of oral cancer cells. *Cancer Med* 2018;**7**:6269−80.
27. Lang M, Berry D, Passecker K, Mesteri I, Bhuju S, Ebner F, et al. HuR small-molecule inhibitor elicits differential effects in adenomatosis polyposis and colorectal carcinogenesis. *Cancer Res* 2017;**77**:2424−38.
28. Nie Y, Xu W, Tian GG, Li X, Guo Y, Liu X, et al. Mechanistic insights into HuR inhibitor MS-444 arresting embryonic development revealed by low-input RNA-seq and storm. *Cell Biol Toxicol* 2022;**38**:1175−97.
29. Pryzbylkowski P, Obajimi O, Keen JC. Trichostatin A and 5 Aza-2′ deoxycytidine decrease estrogen receptor mRNA stability in ER positive MCF7 cells through modulation of HuR. *Breast Cancer Res Treat* 2008;**111**:15−25.
30. Xie Y, Zhang J, Lu B, Bao Z, Zhao J, Lu X, et al. Mefloquine inhibits esophageal squamous cell carcinoma tumor growth by inducing mitochondrial autophagy. *Front Oncol* 2020;**10**:1217.
31. Purhonen J, Banerjee R, Mcdonald AE, Fellman V, Kallijarvi J. A sensitive assay for DNTPs based on long synthetic oligonucleotides, EvaGreen dye and inhibitor-resistant high-fidelity DNA polymerase. *Nucleic Acids Res* 2020;**48**:e87.
32. Jia X, Wang P, Huang C, Zhao D, Wu Q, Lu B, et al. Toosendanin targeting EEF2 impedes topoisomerase I & II protein translation to suppress esophageal squamous cell carcinoma growth. *J Exp Clin Cancer Res* 2023;**42**:97.
33. Martinez MD, Jafari R, Ignatushchenko M, Seki T, Larsson EA, Dan C, et al. Monitoring drug target engagement in cells and tissues using the cellular thermal shift assay. *Science* 2013;**341**:84−7.
34. Jiang Y, Zhao J, Zhang Y, Li K, Li T, Chen X, et al. Establishment of lung cancer patient-derived xenograft models and primary cell lines for lung cancer study. *J Transl Med* 2018;**16**:138.
35. Ohmura S, Marchetto A, Orth MF, Li J, Jabar S, Ranft A, et al. Translational evidence for RRM2 as a prognostic biomarker and therapeutic target in Ewing sarcoma. *Mol Cancer* 2021;**20**:97.
36. Ripin N, Boudet J, Duszczyk MM, Hinniger A, Faller M, Krepl M, et al. Molecular basis for AU-rich element recognition and dimerization by the HuR c-terminal RRM. *Proc Natl Acad Sci U S A* 2019;**116**:2935−44.
37. Jiang M, Jia K, Wang L, Li W, Chen B, Liu Y, et al. Alterations of DNA damage response pathway: biomarker and therapeutic strategy for cancer immunotherapy. *Acta Pharm Sin B* 2021;**11**:2983−94.
38. Goss KL, Koppenhafer SL, Waters T, Terry WW, Wen KK, Wu M, et al. The translational repressor 4E-BP1 regulates RRM2 levels and functions as a tumor suppressor in Ewing sarcoma tumors. *Oncogene* 2021;**40**:564−77.
39. Rasmussen RD, Gajjar MK, Tuckova L, Jensen KE, Maya-Mendoza A, Holst CB, et al. BRCA1-regulated RRM2 expression protects glioblastoma cells from endogenous replication stress and promotes tumorigenicity. *Nat Commun* 2016;**7**:13398.
40. Aye Y, Li M, Long MJ, Weiss RS. Ribonucleotide reductase and cancer: biological mechanisms and targeted therapies. *Oncogene* 2015;**34**:2011−21.
41. Rahman MA, Amin AR, Wang D, Koenig L, Nannapaneni S, Chen Z, et al. RRM2 regulates BCL-2 in head and neck and lung cancers: a potential target for cancer therapy. *Clin Cancer Res* 2013;**19**:3416−28.
42. Tang Q, Wu L, Xu M, Yan D, Shao J, Yan S. Osalmid, a novel identified RRM2 inhibitor, enhances radiosensitivity of esophageal cancer. *Int J Radiat Oncol Biol Phys* 2020;**108**:1368−79.
43. Perrault EN, Shireman JM, Ali ES, Lin P, Preddy I, Park C, et al. Ribonucleotide reductase regulatory subunit M2 drives glioblastoma

TMZ resistance through modulation of dNTP production. *Sci Adv* 2023;**9**:eade7236.
44. Wu X, Xu L. The RNA-binding protein HuR in human cancer: a friend or foe? *Adv Drug Deliv Rev* 2022;**184**:114179.
45. Fan Z, Wu C, Chen M, Jiang Y, Wu Y, Mao R, et al. The generation of PD-L1 and PD-L2 in cancer cells: from nuclear chromatin reorganization to extracellular presentation. *Acta Pharm Sin B* 2022;**12**:1041−53.
46. Yang X, Shang P, Yu B, Jin Q, Liao J, Wang L, et al. Combination therapy with miR34a and doxorubicin synergistically inhibits Dox-resistant breast cancer progression *via* down-regulation of snail through suppressing Notch/NF-kappaB and RAS/RAF/MEK/ERK signaling pathway. *Acta Pharm Sin B* 2021;**11**:2819−34.
47. Chen CY, Shyu AB. Mechanisms of deadenylation-dependent decay. *Wiley Interdiscip Rev RNA* 2011;**2**:167−83.
48. Li D, Yu W, Lai M. Towards understandings of serine/arginine-rich splicing factors. *Acta Pharm Sin B* 2023;**13**:3181−207.
49. George J, Li Y, Kadamberi IP, Parashar D, Tsaih SW, Gupta P, et al. RNA-binding protein FXR1 drives cMYC translation by recruiting eIF4F complex to the translation start site. *Cell Rep* 2023;**42**:112228.
50. Sun X, Hu Y, Wu J, Shi L, Zhu L, Xi PW, et al. RBMS2 inhibits the proliferation by stabilizing p21 mRNA in breast cancer. *J Exp Clin Cancer Res* 2018;**37**:298.
51. Wu Q, Liu F, Ge M, Laster KV, Wei L, Du R, et al. BRD4 drives esophageal squamous cell carcinoma growth by promoting RCC2 expression. *Oncogene* 2022;**41**:347−60.
52. Liu F, Wu Q, Han W, Laster K, Hu Y, Ma F, et al. Targeting integrin $\alpha v\beta 3$ with indomethacin inhibits patient-derived xenograft tumor growth and recurrence in oesophageal squamous cell carcinoma. *Clin Transl Med* 2021;**11**:e548.
53. D'Agostino VG, Sighel D, Zucal C, Bonomo I, Micaelli M, Lolli G, et al. Screening approaches for targeting ribonucleoprotein complexes: a new dimension for drug discovery. *SLAS Discov* 2019;**24**:314−31.
54. Mehta M, Raguraman R, Ramesh R, Munshi A. RNA binding proteins (RBPs) and their role in DNA damage and radiation respons in cancer. *Adv Drug Deliv Rev* 2022;**191**:114569.
55. Kim SJ, Ju JS, Kang MH, Eun JW, Kim YH, Raninga PV, et al. RNA-binding protein NONO contributes to cancer cell growth and confers drug resistance as a theranostic target in TNBC. *Theranostics* 2020;**10**:7974−92.